Electronic Supplementary Information for:

Ethylene Oligomerization in Metal–Organic Frameworks Bearing Nickel(II) Bipyridine Complexes

Miguel I. Gonzalez,[a] Julia Oktawiec,[a] and Jeffrey R. Long*[abc]

[a]Department of Chemistry, University of California, Berkeley, California, 94720-1462, USA.
[b]Department of Chemical and Biomolecular Engineering, University of California, Berkeley, California, 94720-1462, USA.
[c]Materials Sciences Division, Lawrence Berkeley National Laboratory, Berkeley, California 94720, United States, 94720, USA.

Table of Contents

Single-Crystal X-ray Diffraction Data

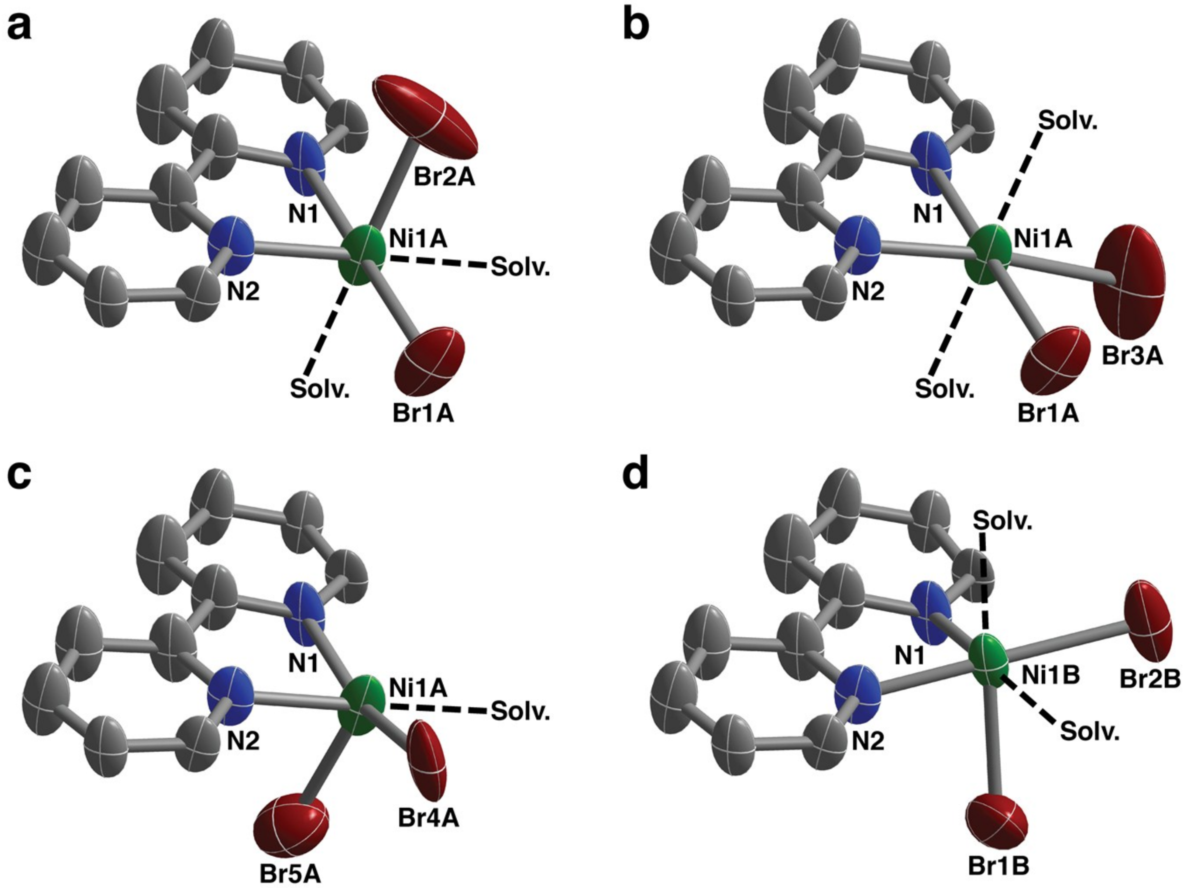

a		b		c		d	
occupancy	40%	occupancy	12%	occupancy	12%	occupancy	30%
Ni1A–N1	2.021(11) Å	Ni1A–N1	2.021(11) Å	Ni1A–N1	2.021(11) Å	Ni1B–N1	2.095(14) Å
Ni1A–N2	2.078(11) Å	Ni1A–N2	2.078(11) Å	Ni1A–N2	2.078(11) Å	Ni1B–N2	2.009(14) Å
Ni1A–Br1A	2.466(6) Å	Ni1A–B1A	2.466(6) Å	Ni1A–Br4A	2.76(2) Å	Ni1A–Br1B	2.584(14) Å
Ni1A–Br2A	2.474(11) Å	Ni1A–Br3A	2.55(3) Å	Ni1A–Br5A	2.58(3)	Ni1A–Br2B	2.478(12)
Br1A–Ni1A–Br2A	94.8(3)°	Br1A–Ni1A–Br3A	86.2(6)°	Br4A–Ni1A–Br5A	118.4(8)°	Br1B–Ni1B–Br2B	95.7(5)°
Br1A–Ni1A–N2	80.0(4)°	Br1A–Ni1A–N2	80.0(4)°	Br4A–Ni1A–N2	89.3(5)°	Br1B–Ni1B–N1	90.4(6)°
Br2A–Ni1A–N1	96.8(4)°	Br3A–Ni1A–N1	84.0(7)°	Br5A–Ni1A–N1	95.0(7)°	Br1B–Ni1B–N2	82.5(5)°
Br2A–Ni1A–N2	82.4(5)°			Br5A–Ni1A–N2	95.8(7)°	Br2B–Ni1B–N1	81.7(5)°

Figure S1. Structures and selected parameters of the (bpy)$NiBr_2$ complexes in $Zr_6O_4(OH)_4(bpydc)_6(NiBr_2)_{5.64}$ at 100 K as determined by single-crystal X-ray diffraction; green, dark red, blue, and gray spheres represent Ni, Br, N, and C atoms, respectively. The Ni^{II} centers are disordered over two positions. One position (Ni1A) is assigned to have pseudooctahedral (**a** and **b**) and square pyramidal (**c**) geometries, while the other positon (Ni1B) is pseudooctahedral (**d**). Coordinating solvent molecules that complete the nickel coordination spheres could not be resolved, due to disorder and weak scattering compared to the Br^- ligands. Hydrogen atoms are omitted for clarity.

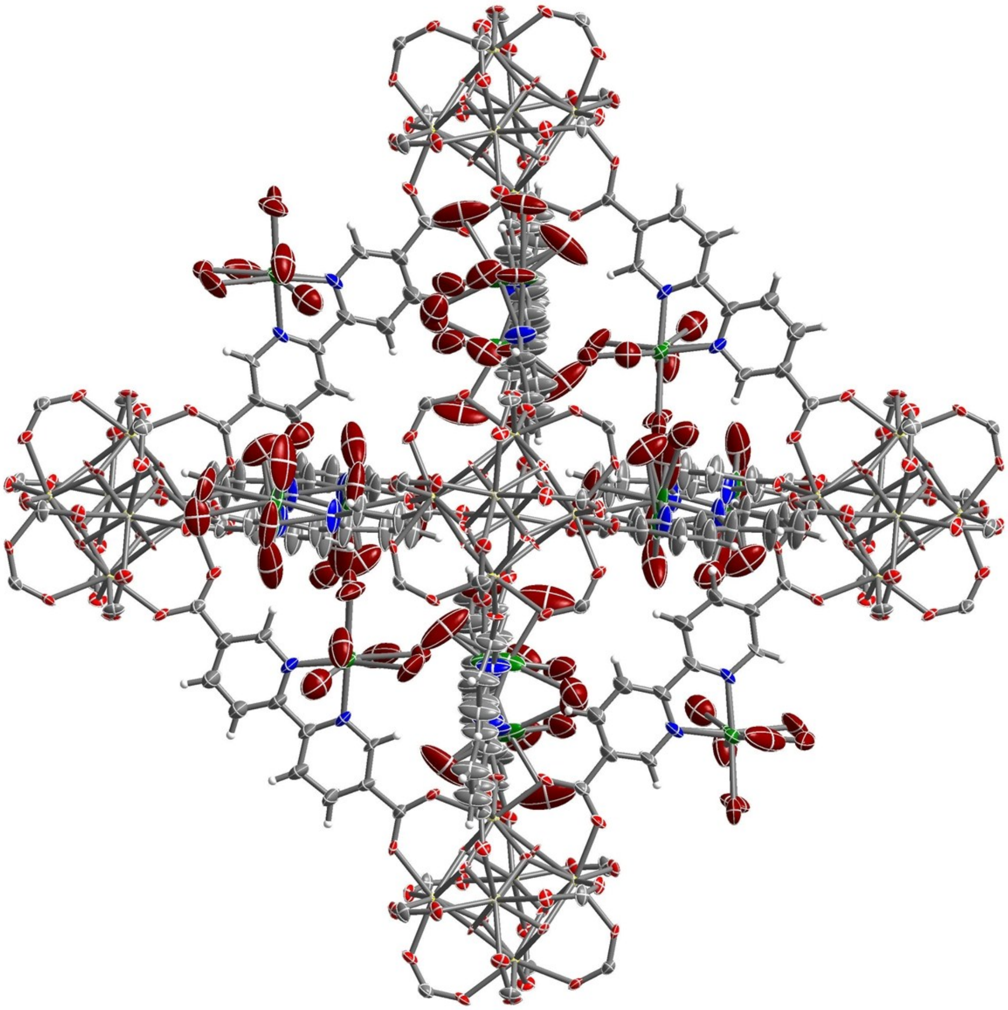

Figure S2. Thermal ellipsoid plot of $Zr_6O_4(OH)_4(bpydc)_6(NiBr_2)_{5.64}$ at 100 K drawn at 50% probability level as determined by single crystal X-ray diffraction; yellow, green, dark red, red, blue, gray, and white ellipsoids represent Zr, Ni, Br, O, N, C, and H atoms, respectively.

Table S1. Crystallographic Data for $Zr_6O_4(OH)_4(bpydc)_6(NiBr_2)_{5.64}$

Formula	$Zr_6O_{30.56}C_{67.68}N_{11.28}H_{33.84}Ni_{5.64}Br_{11.28}$
Temperature (K)	100(2)
Crystal System	Cubic
Space Group	$Pa\bar{3}$
a, b, c (Å)	26.2758(8)
α, β, γ (°)	90
V (Å^3)	18141.3(17)
Z	4
Radiation, λ (Å)	Synchrotron, 0.8856
2Θ Range for Data Collection (°)	4.320 to 59.612
Completeness to 2Θ	100.0% (2Θ = 59.612°)
Data / Restraints / Parameters	4662 / 705 / 278
Goodness of Fit on F^2	1.151
$R1^a$, $wR2^b$ ($I>2\sigma(I)$)	0.0651, 0.2002
$R1^a$, $wR2^b$ (all data)	0.0715, 0.2046
Largest Diff. Peak and Hole (e Å^{-3})	1.044 and –0.677

$^aR_1 = \sum||F_o| - |F_c||/\sum|F_o|$. $^bwR_2 = \{\sum[w(F_o^2 - F_c^2)^2]/\sum[w(F_o^2)^2]\}^{1/2}$.

Powder X-ray Diffraction Data

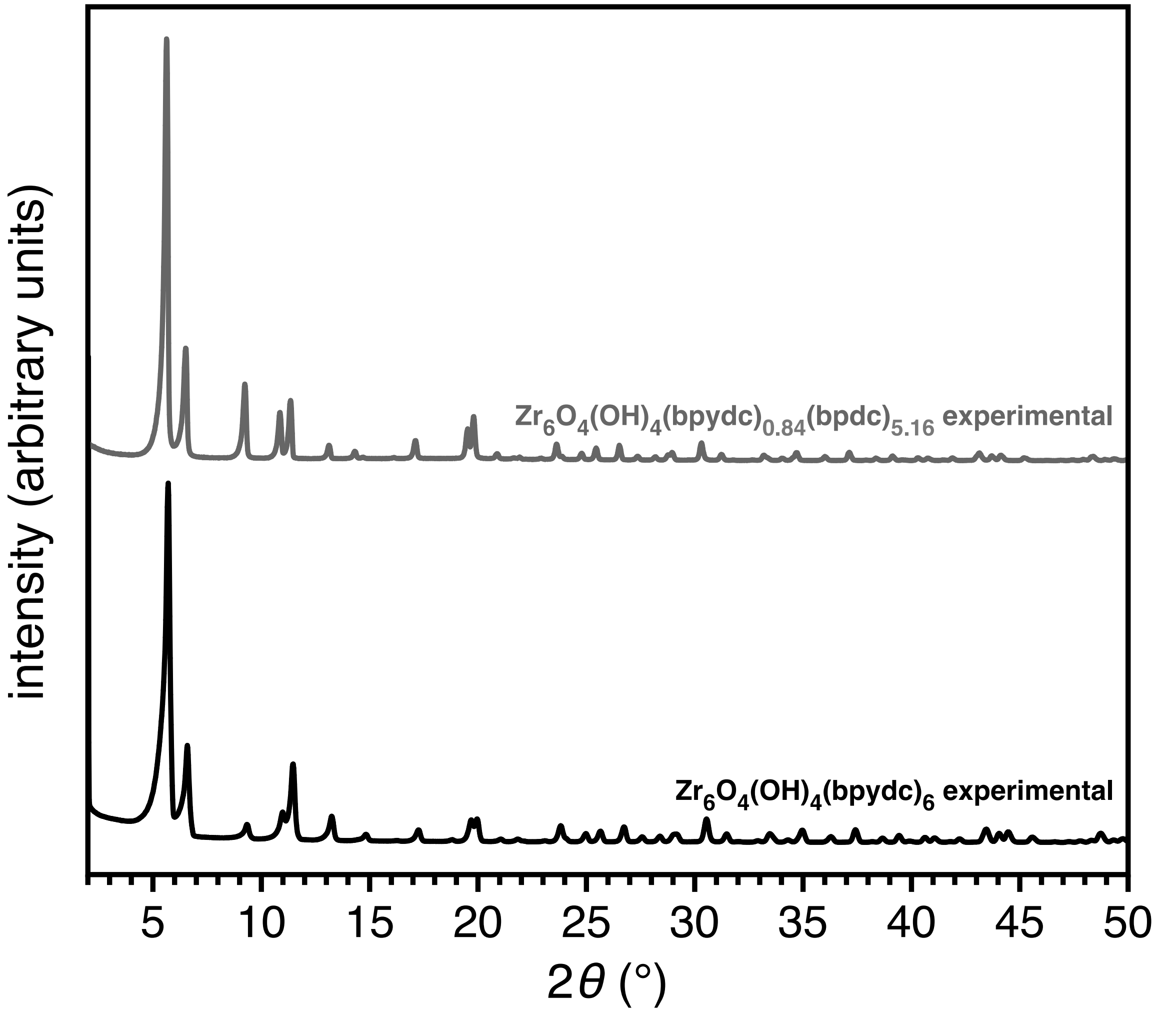

Figure S3. Comparison of the powder X-ray diffraction patterns for $Zr_6O_4(OH)_4(bpydc)_6$ (**1**; black) and $Zr_6O_4(OH)_4(bpydc)_{0.84}(bpdc)_{5.16}$ (**2**; light gray) at 298 K with a wavelength of 1.5418 Å.

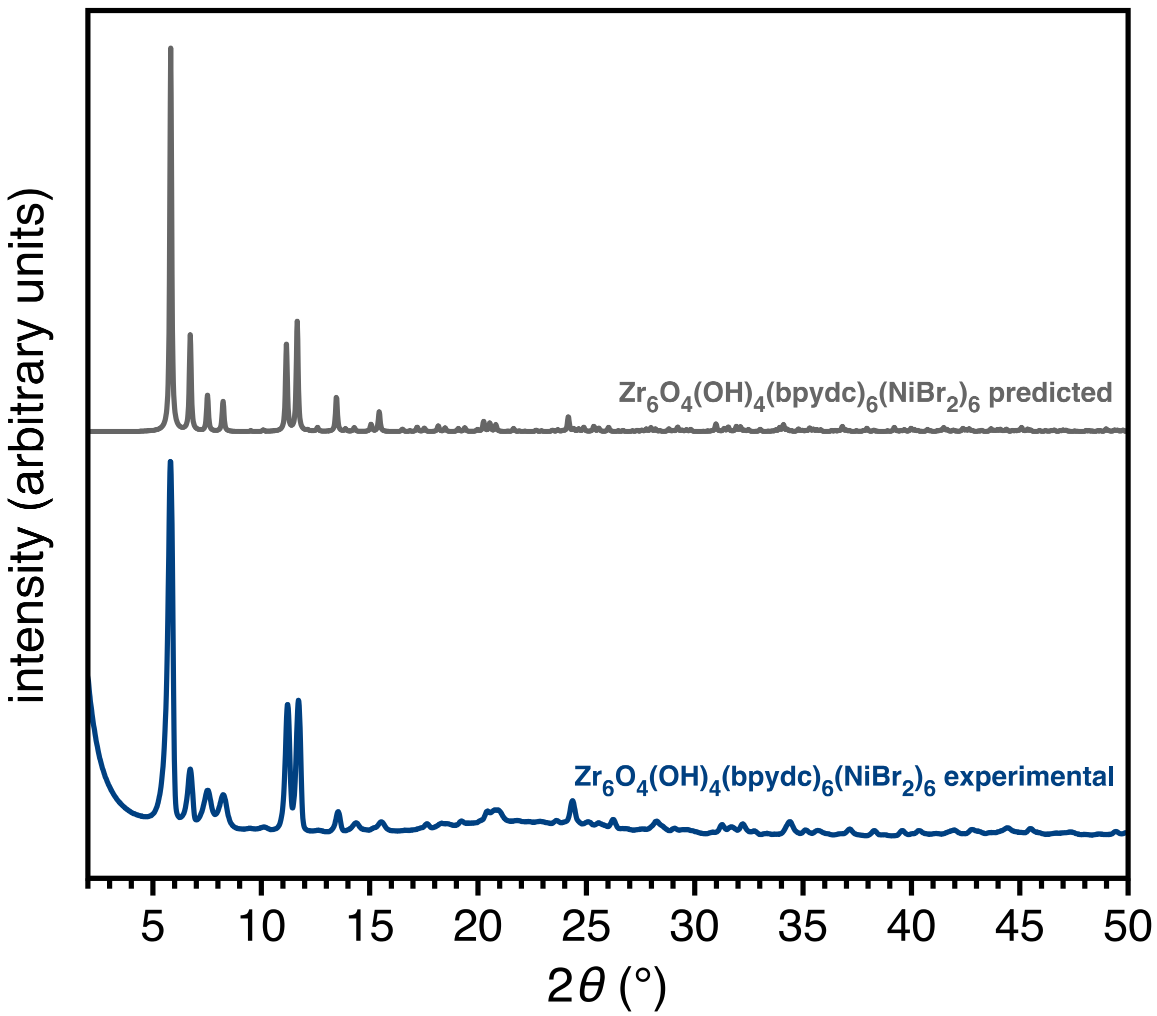

Figure S4. Comparison of the predicted (light gray) and experimental (blue) powder X-ray diffraction patterns for $Zr_6O_4(OH)_4(bpydc)_6(NiBr_2)_6$ (**1**$(NiBr_2)_6$) at 298 K with a wavelength of 1.5418 Å.

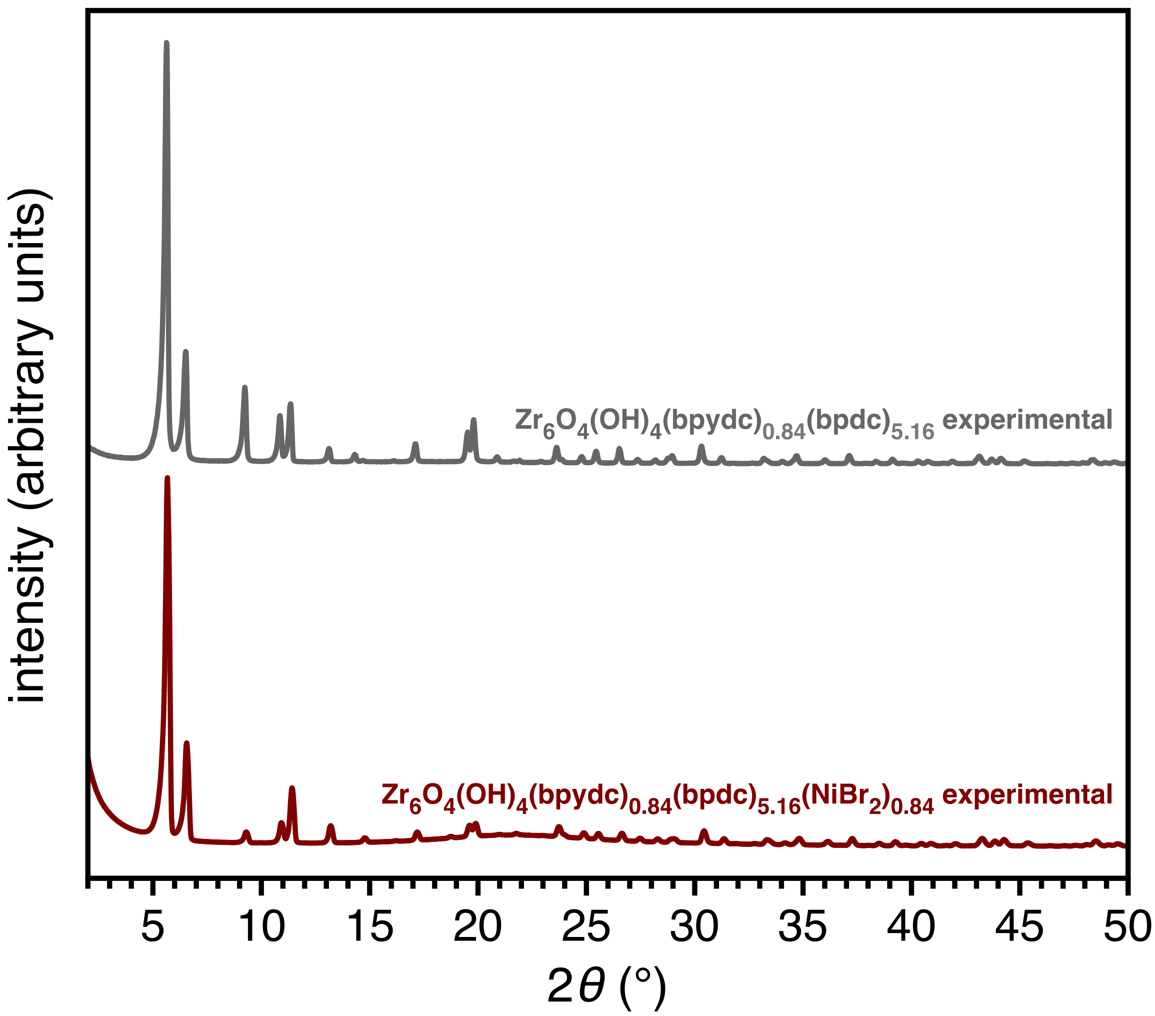

Figure S5. Comparison of the powder X-ray diffraction patterns for $Zr_6O_4(OH)_4(bpydc)_{0.84}(bpdc)_{5.16}$ (**2**; light gray) and $Zr_6O_4(OH)_4(bpydc)_{0.84}(bpdc)_{5.16}(NiBr_2)_{0.84}$ (**2**$(NiBr_2)_{0.84}$; red) at 298 K with a wavelength of 1.5418 Å.

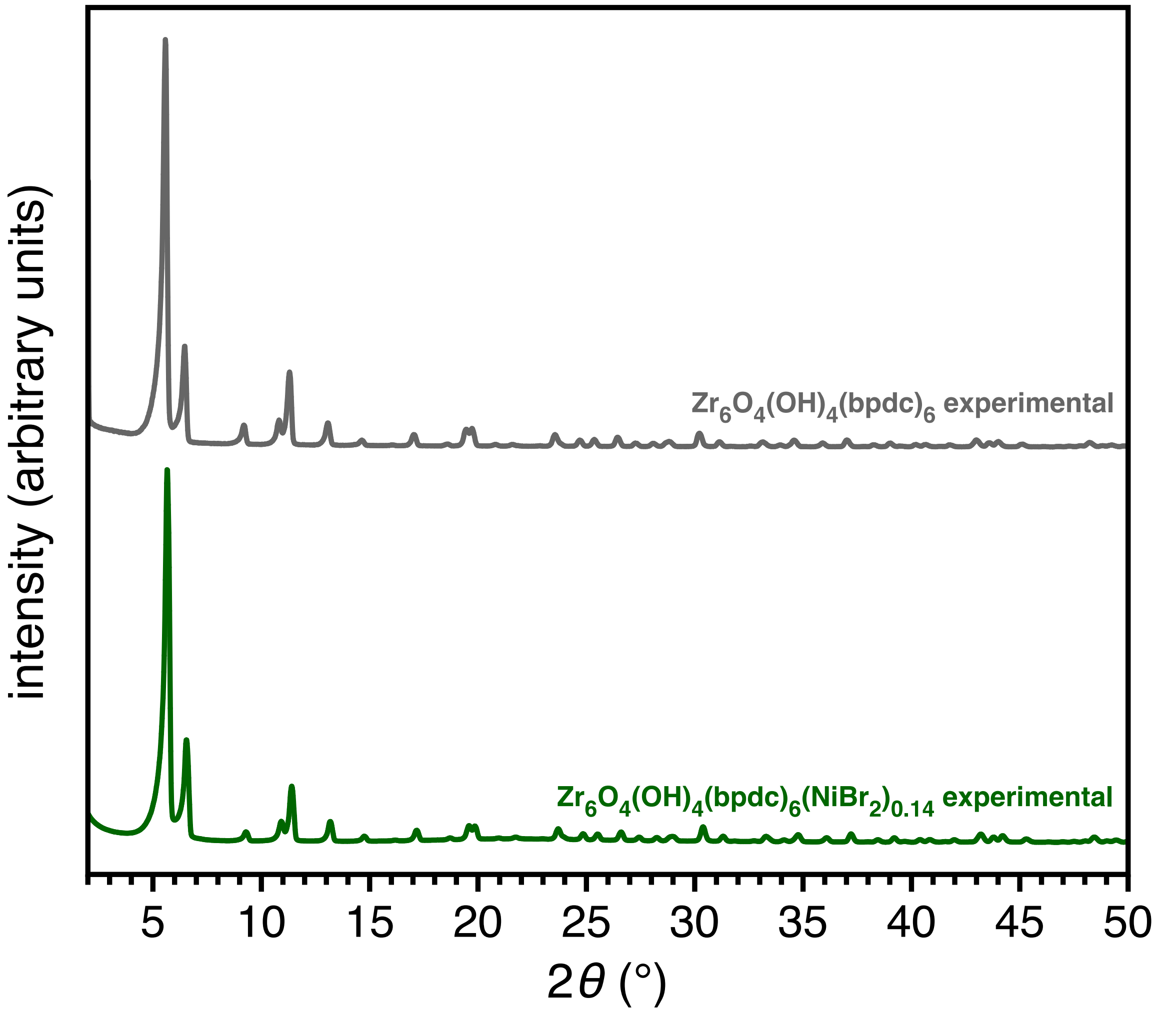

Figure S6. Comparison of the powder X-ray diffraction patterns for $Zr_6O_4(OH)_4(bpdc)_6$ (**3**; light gray) and $Zr_6O_4(OH)_4(bpdc)_6(NiBr_2)_{0.14}$ (**3**$(NiBr_2)_{0.14}$; green) at 298 K with a wavelength of 1.5418 Å.

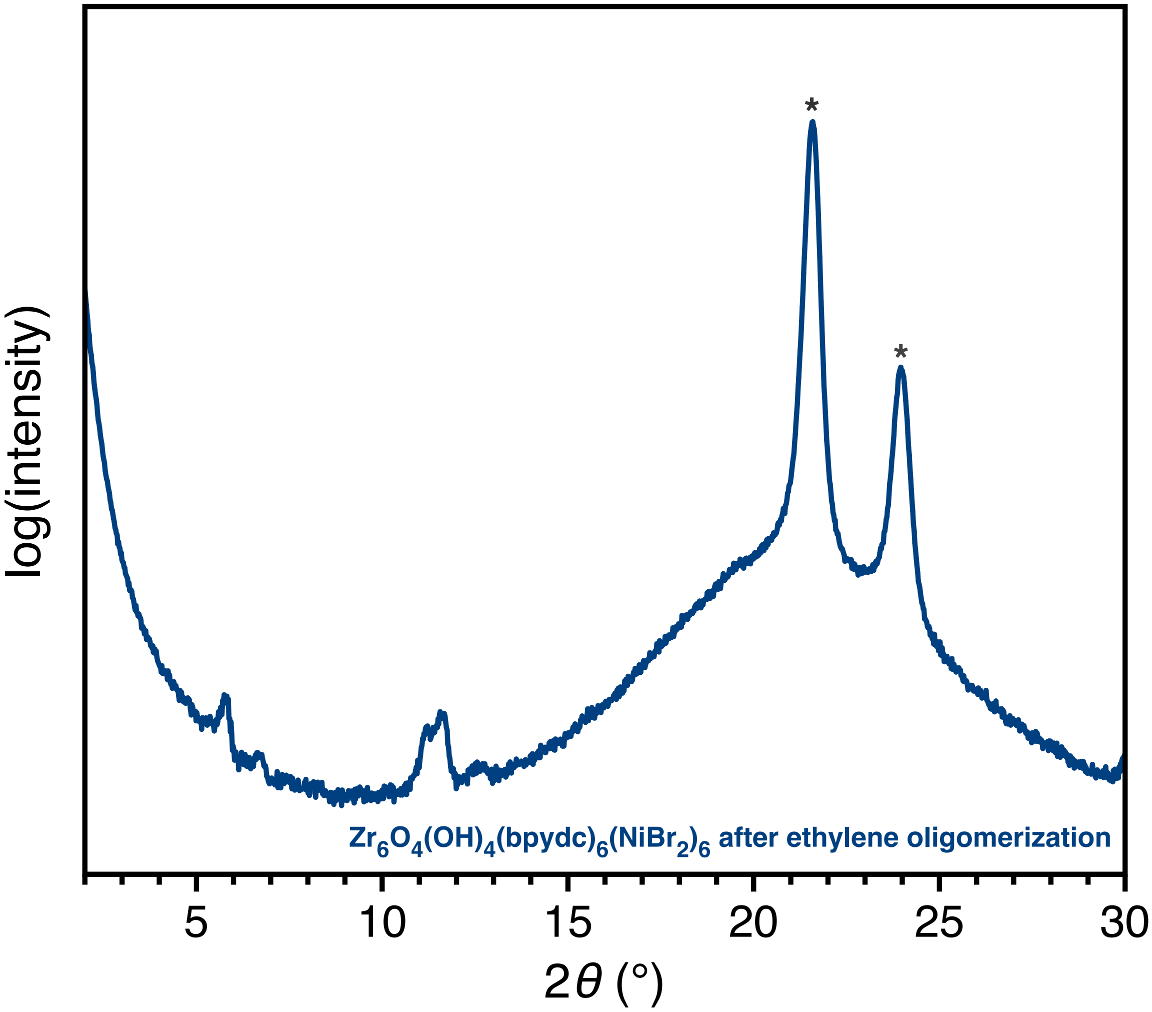

Figure S7. Powder X-ray diffraction pattern (at 298 K) of the solid recovered from an ethylene oligomerization reaction with $Zr_6O_4(OH)_4(bpydc)_6(NiBr_2)_6$ (**1**$(NiBr_2)_6$; blue) taken at 298 K with a wavelength of 1.5418 Å. Peaks corresponding to polyethylene are marked by gray asterisks. Note that the intensity is plotted on a logarithmic scale because the metal–organic framework was found to be embedded in a considerable amount of polyethylene (~5 mg metal–organic framework in 1 g of polyethylene).

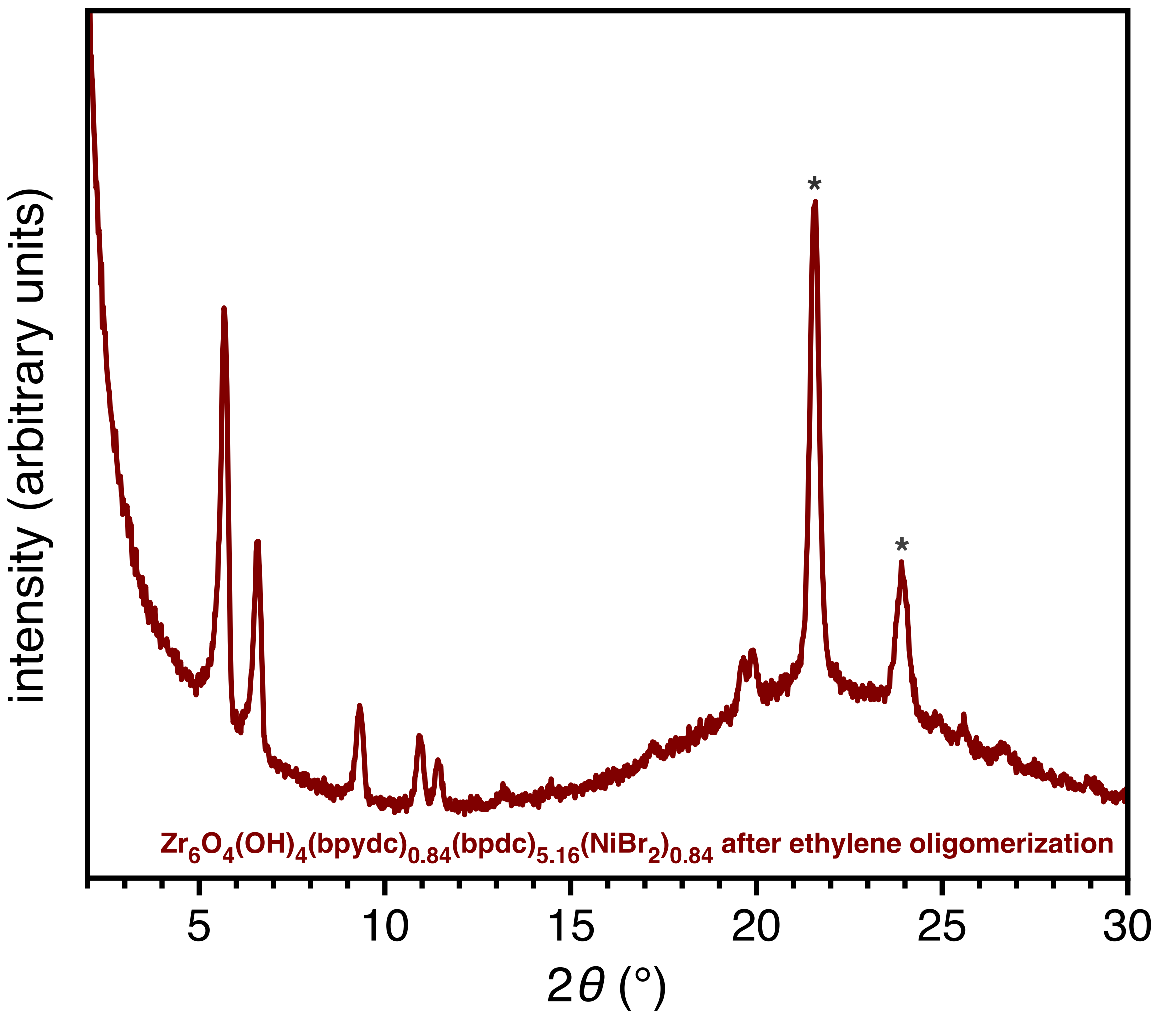

Figure S8. Powder X-ray diffraction pattern of the solid recovered from an ethylene oligomerization reaction with $Zr_6O_4(OH)_4(bpydc)_{0.84}(bpdc)_{5.16}(NiBr_2)_{0.84}$ (**2**$(NiBr_2)_{0.84}$; red) taken at 298 K with a wavelength of 1.5418 Å. Peaks corresponding to polyethylene are marked by gray asterisks.

Table S2. Unit cell parameters determined *via* Pawley fitting of powder X-ray diffraction data.

	$1(NiBr_2)_6$	**$2(NiBr_2)_{0.84}$**	**$3(NiBr_2)_{0.13}$**
Space group	$Pa\bar{3}$	$Fm\bar{3}m$	$Fm\bar{3}m$
a (Å)	26.048(2)	26.7418(6)	26.7836(6)
V (Å^3)	17674(4)	19123.7(14)	19213.4(12)
R_{exp}	0.310	0.364	0.266
R_{wp}	3.280	3.068	3.743
R_{p}	1.933	2.028	2.639
Wavelength (Å)	1.5418	1.5418	1.5418
Temperature (K)	298	298	298

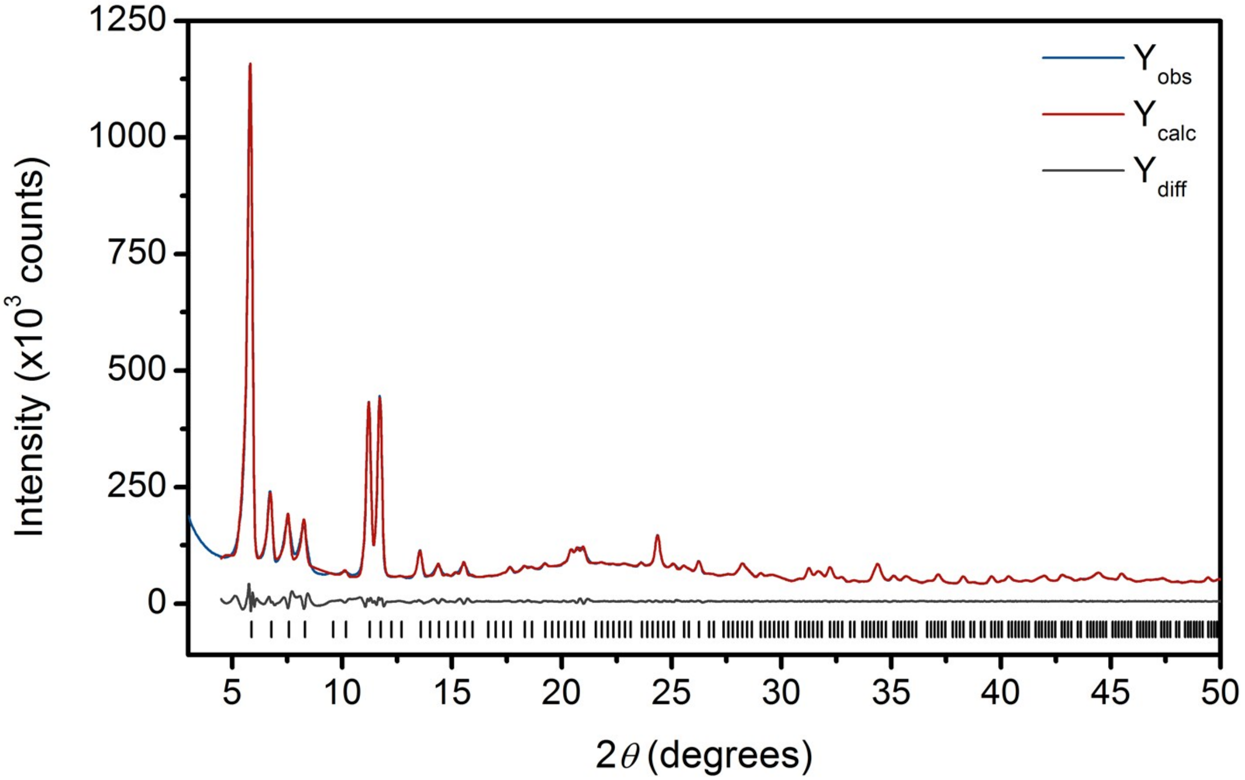

Figure S9. Pawley refinement of **1**$(NiBr_2)_6$ from 2° to 50°, as implemented by TOPAS-Academic.[1] The experimental powder pattern of **1**$(NiBr_2)_6$ was taken on a Bruker D8 Advance powder X-ray diffractometer at 298 K with a wavelength of 1.5418 Å. Blue, red, and gray lines represent experimental data, calculated fits, and the difference between the two, respectively; black tick marks represent calculated Bragg peak positions. The broad hump observed at approximately 20–25° is due to diffuse scattering of the borosilicate capillary the sample was packed into.

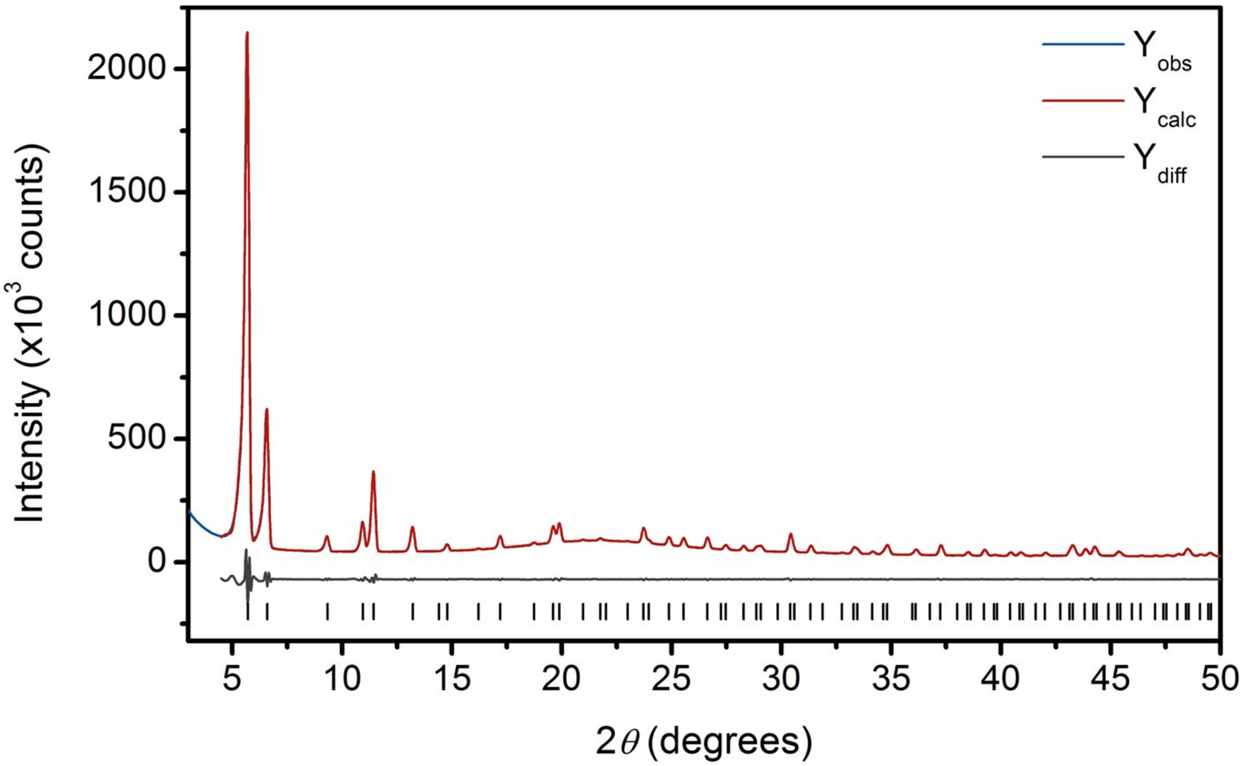

Figure S10. Pawley refinement of **2**$(NiBr_2)_{0.84}$ from 2° to 50°, as implemented by TOPAS-Academic.[1] The experimental powder pattern of **2**$(NiBr_2)_{0.84}$ was taken on a Bruker D8 Advance powder X-ray diffractometer at 298 K with a wavelength of 1.5418 Å. Blue, red, and gray lines represent experimental data, calculated fits, and the difference between the two, respectively; black tick marks represent calculated Bragg peak positions. The broad hump observed at approximately 20–25° is due to diffuse scattering of the borosilicate capillary the sample was packed into.

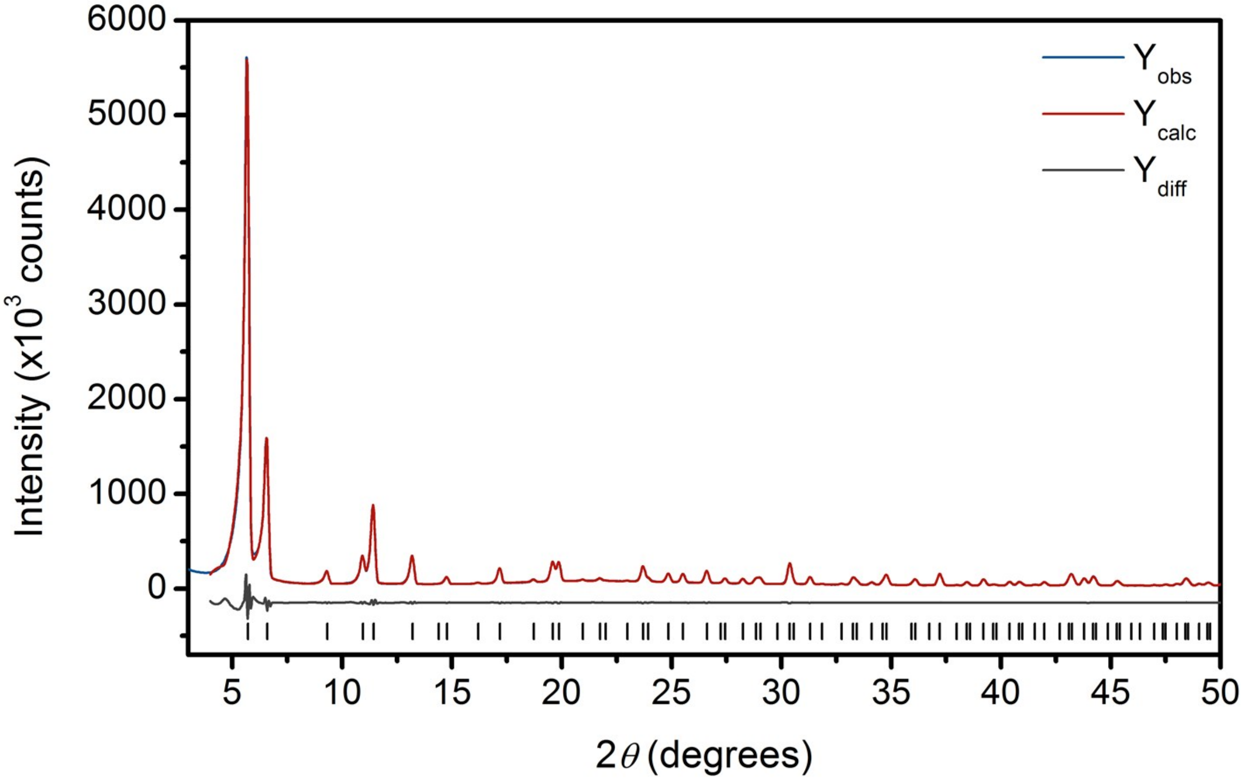

Figure S11. Pawley refinement of **3**$(NiBr_2)_{0.14}$ from 2° to 50°, as implemented by TOPAS-Academic.[1] The experimental powder pattern of **3**$(NiBr_2)_{0.14}$ was taken on a Bruker D8 Advance powder X-ray diffractometer at 298 K with a wavelength of 1.5418 Å. Blue, red, and gray lines represent experimental data, calculated fits, and the difference between the two, respectively; black tick marks represent calculated Bragg peak positions. The broad hump observed at approximately 20–25° is due to diffuse scattering of the borosilicate capillary the sample was packed into.

Low-pressure Gas Adsorption Isotherms

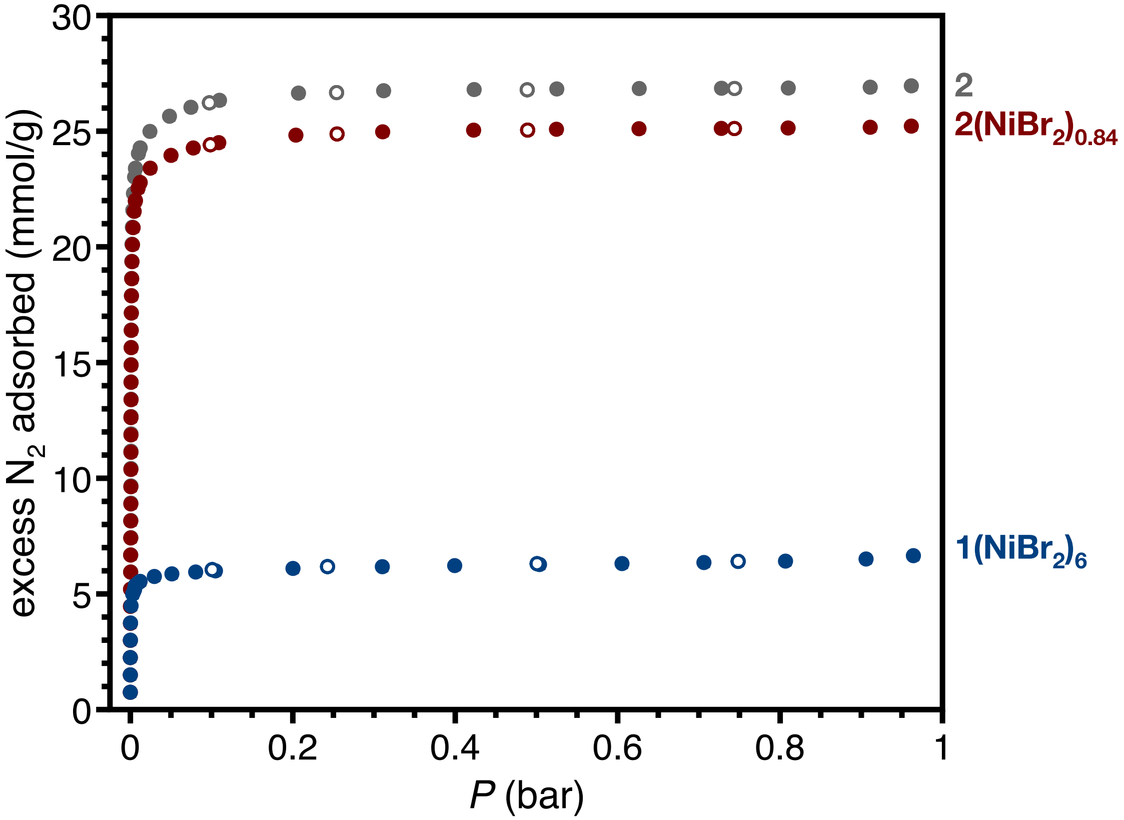

Figure S12. Low-pressure N_2 adsorption isotherms for **2**, **2**$(NiBr_2)_{0.84}$, and **1**$(NiBr_2)_6$ at 77 K. Filled circles represent adsorption, while open circles represent desorption.

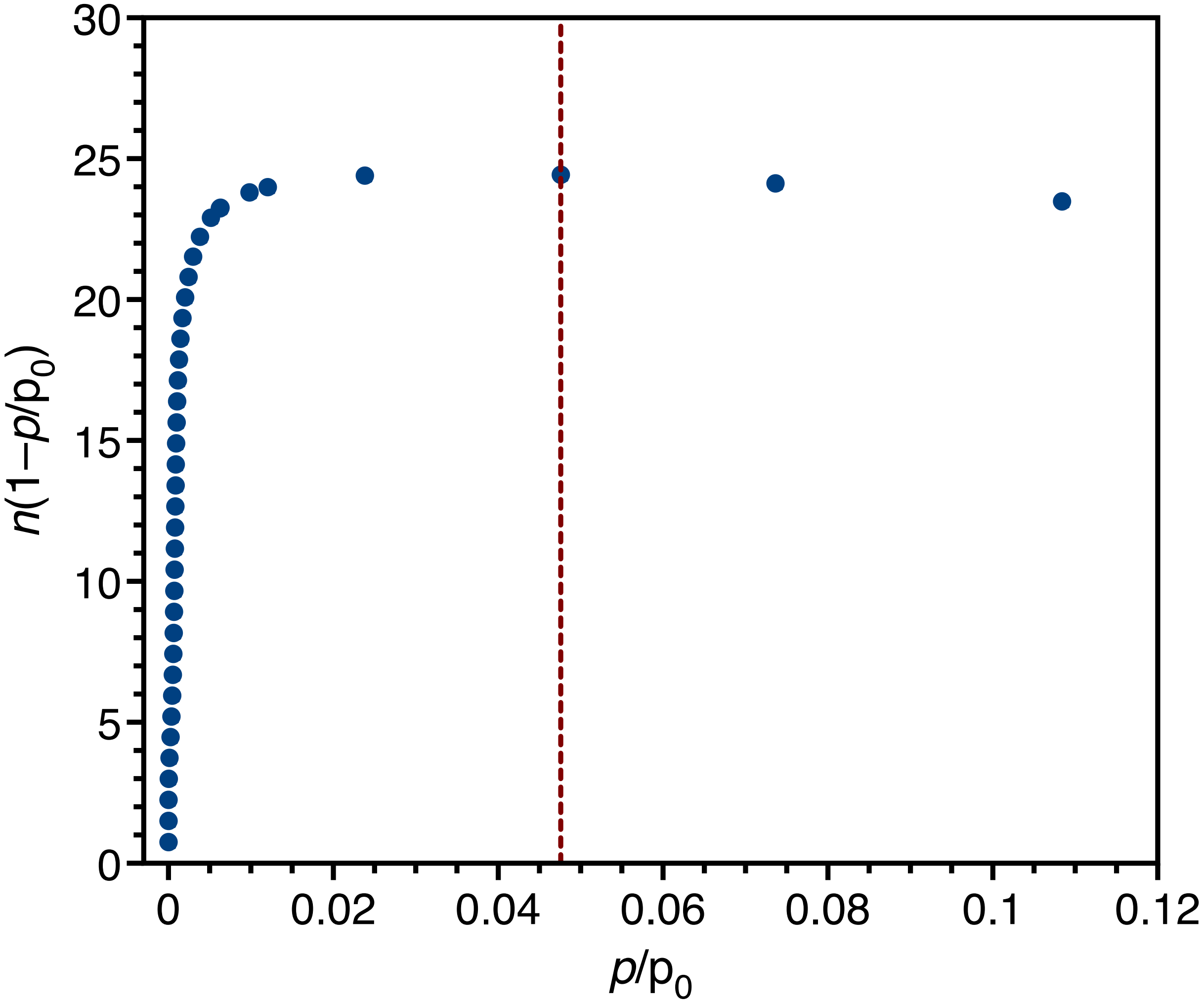

Figure S13. Plot of $n(1-p/p_0)$ vs. p/p_0 for **2** to determine the maximum p/p_0 used in the BET linear fit according to the first BET consistency criterion.[2]

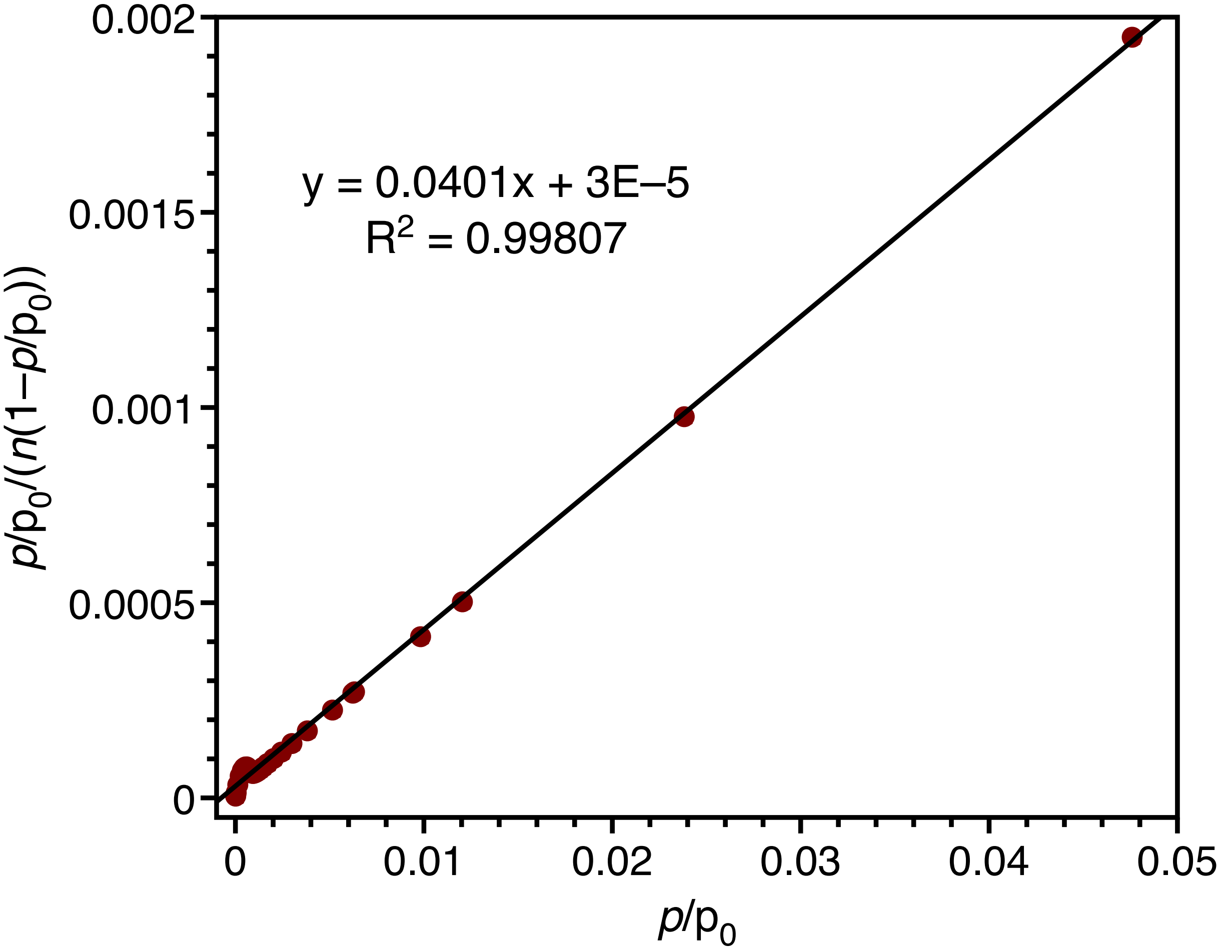

Figure S14. Plot of $p/p_0/(n(1-p/p_0))$ vs. p/p_0 for **2** to determine the BET surface area.[2] The slope of the best fit line for $p/p_0 < 0.03$ is 0.0401, and the y-intercept is 3×10^{-5}, which satisfies the second BET consistency criterion. This results in a saturation capacity of 24.9 mmol/g and a BET surface area of 2430 ± 20 m^2/g.

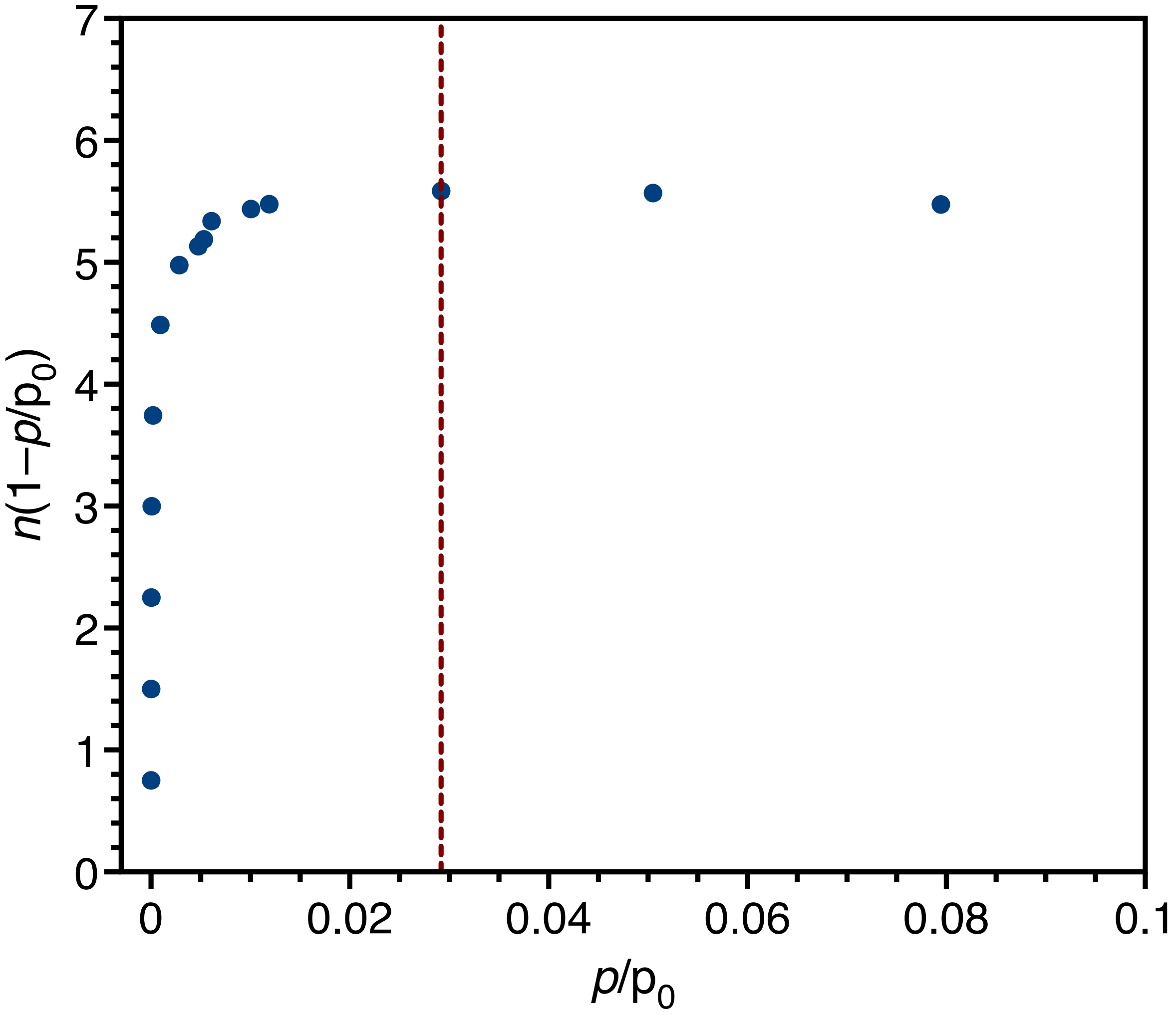

Figure S15. Plot of $n(1–p/p_0)$ vs. p/p_0 for **1**$(NiBr_2)_6$ to determine the maximum p/p_0 used in the BET linear fit according to the first BET consistency criterion.[2]

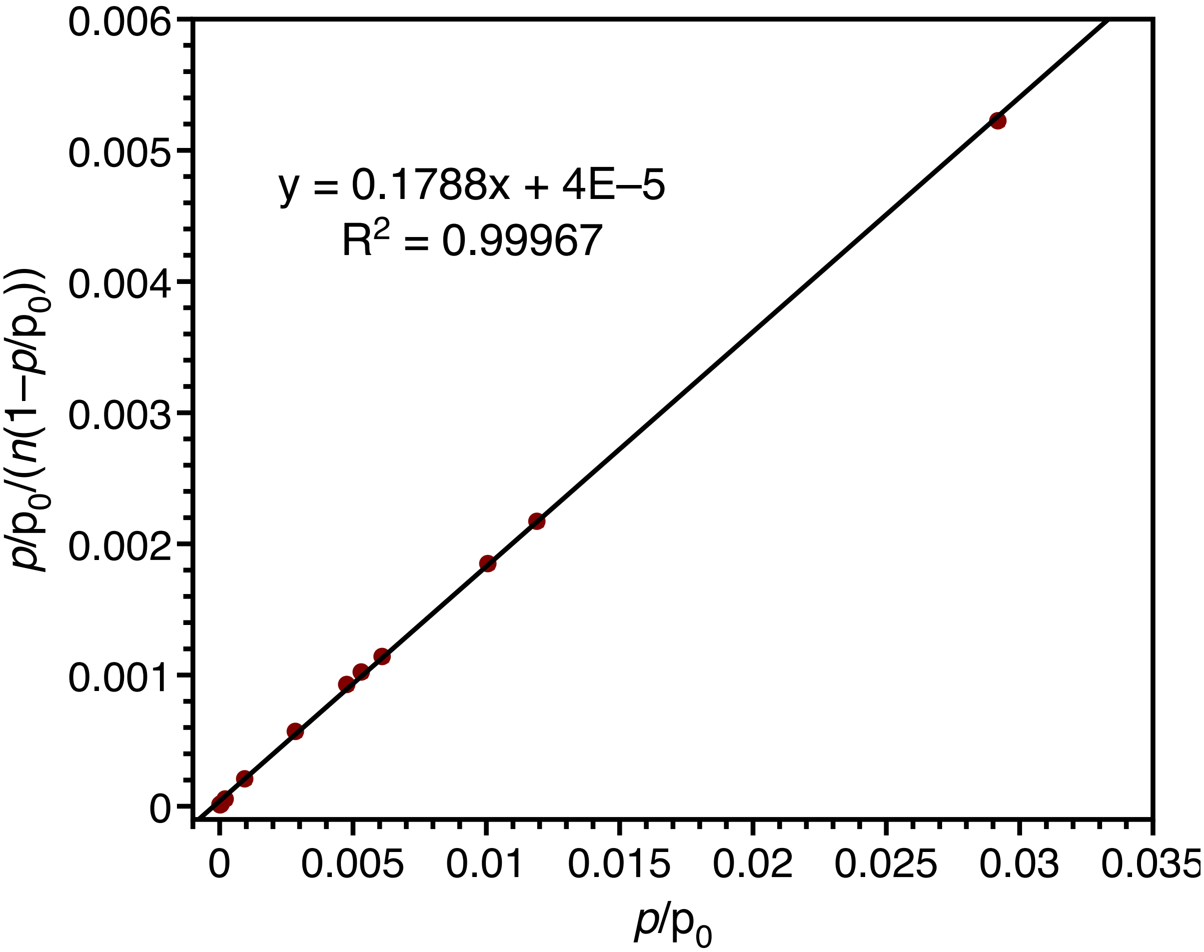

Figure S16. Plot of $p/\mathrm{p}_0/(n(1–p/\mathrm{p}_0))$ vs. p/p_0 for **1**$(\mathrm{NiBr_2})_6$ to determine the BET surface area.[2] The slope of the best fit line for $p/\mathrm{p}_0 < 0.03$ is 0.1788, and the y-intercept is 4×10^{-5}, which satisfies the second BET consistency criterion. This results in a saturation capacity of 5.6 mmol/g and a BET surface area of 545 ± 3 $\mathrm{m^2/g}$.

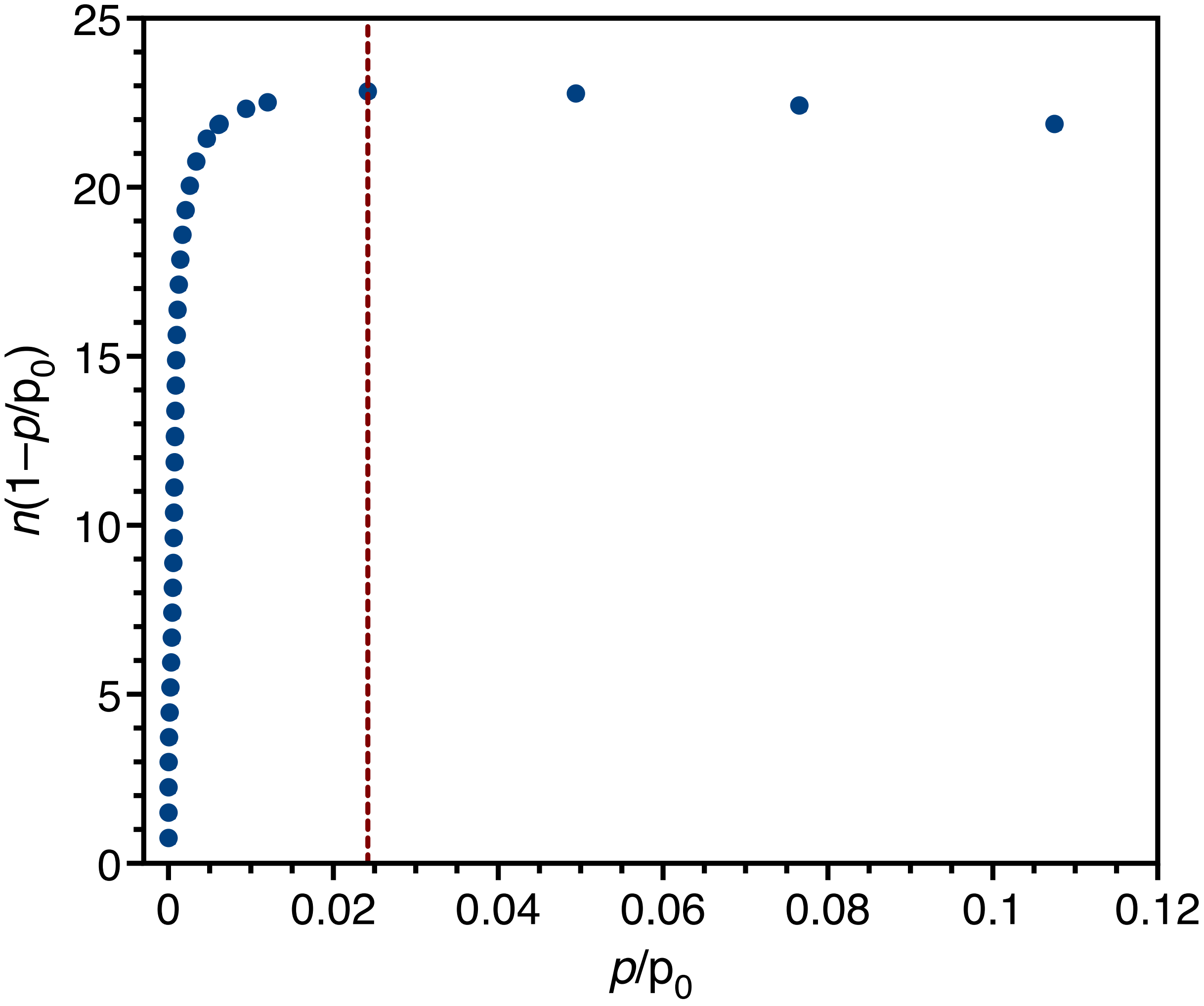

Figure S17. Plot of $n(1-p/p_0)$ vs. p/p_0 for **2**$(NiBr_2)_{0.84}$ to determine the maximum p/p_0 used in the BET linear fit according to the first BET consistency criterion.[2]

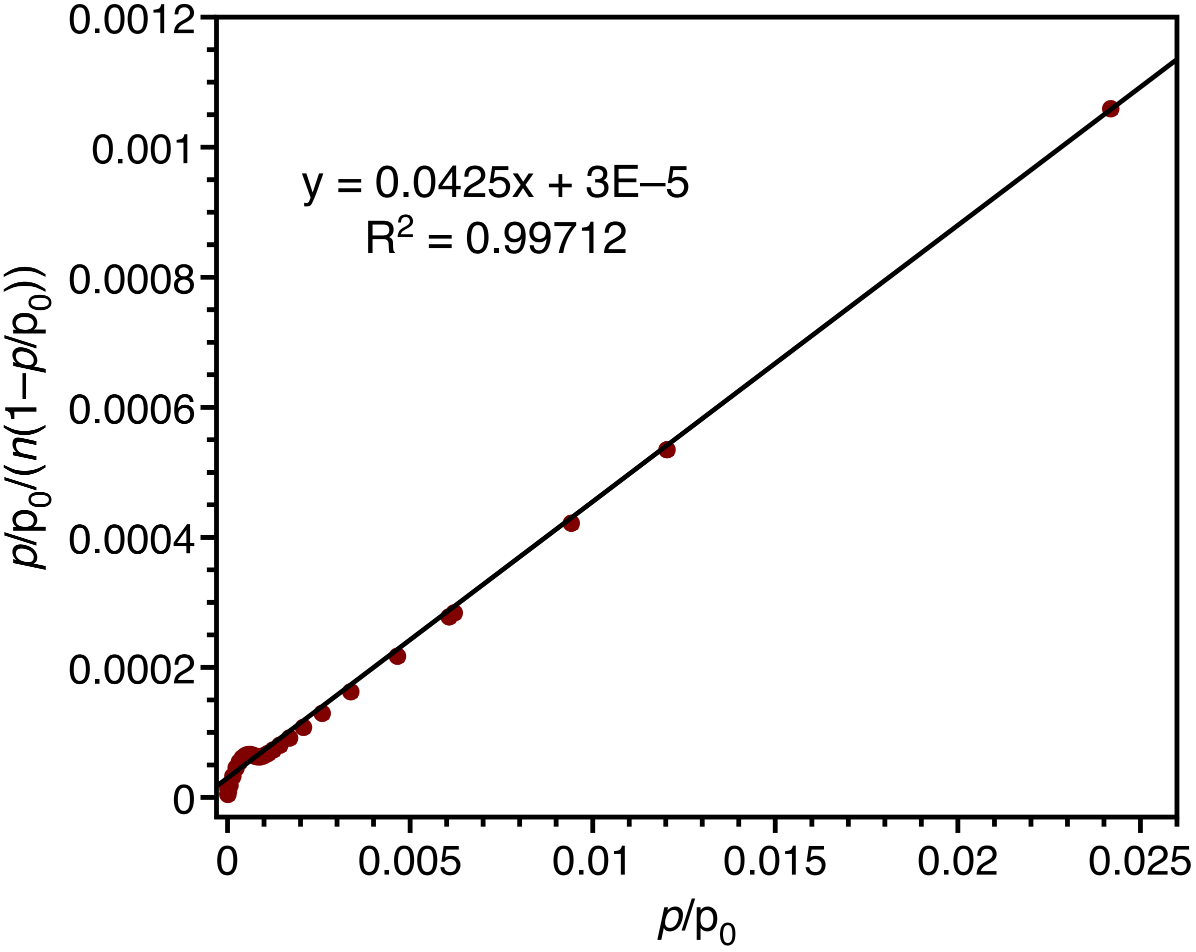

Figure S18. Plot of $p/p_0/(n(1–p/p_0))$ vs. p/p_0 for **2**$(NiBr_2)_{0.84}$ to determine the BET surface area.[2] The slope of the best fit line for $p/p_0 < 0.03$ is 0.0425, and the y-intercept is 3×10^{-5}, which satisfies the second BET consistency criterion. This results in a saturation capacity of 23.5 mmol/g and a BET surface area of 2300 ± 20 m^2/g.

Thermogravimetric Analyses

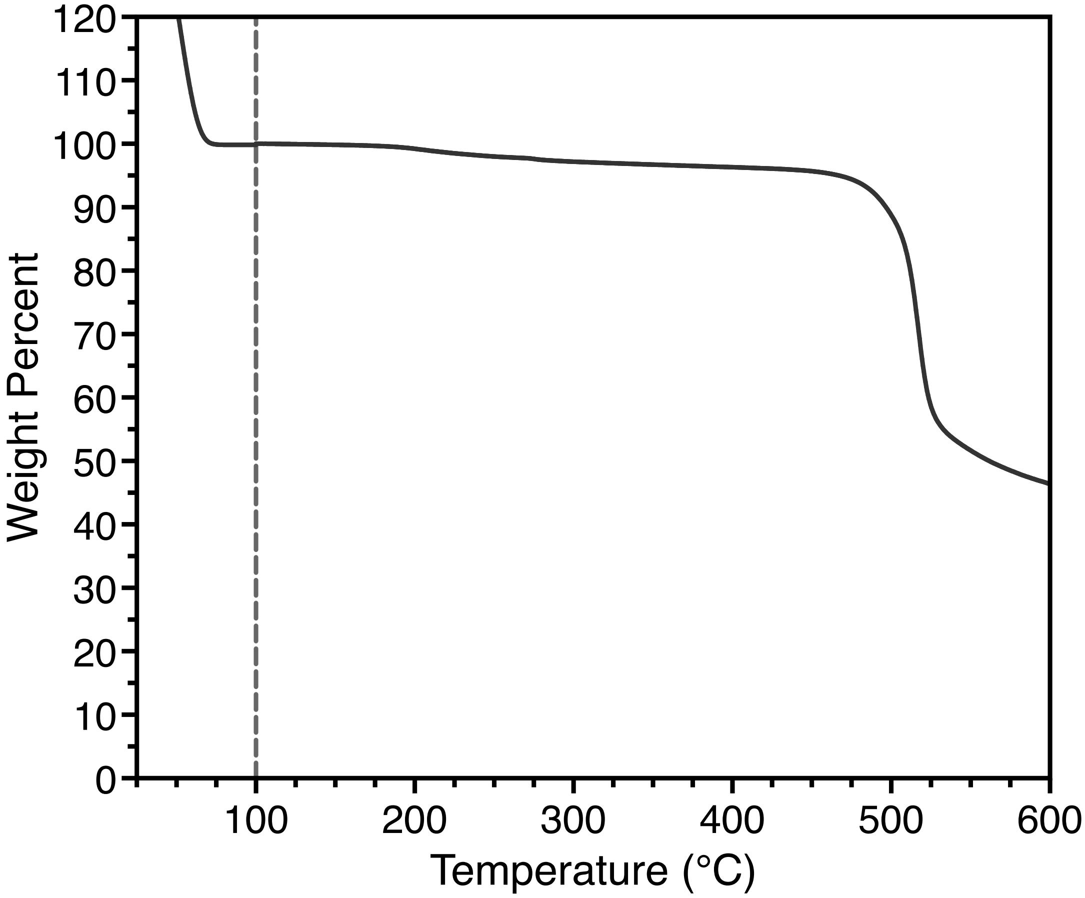

Figure S19. Thermogravimetric analysis of a slurry of **2** in n-hexane. The sample was heated at a ramp rate of 1 °C/min. to 100 °C, then held at this temperature for 1 hour (dashed gray line) to evaporate any remaining n-hexane. The sample was then heated at a ramp rate of 1 °C/min. to 600 °C.

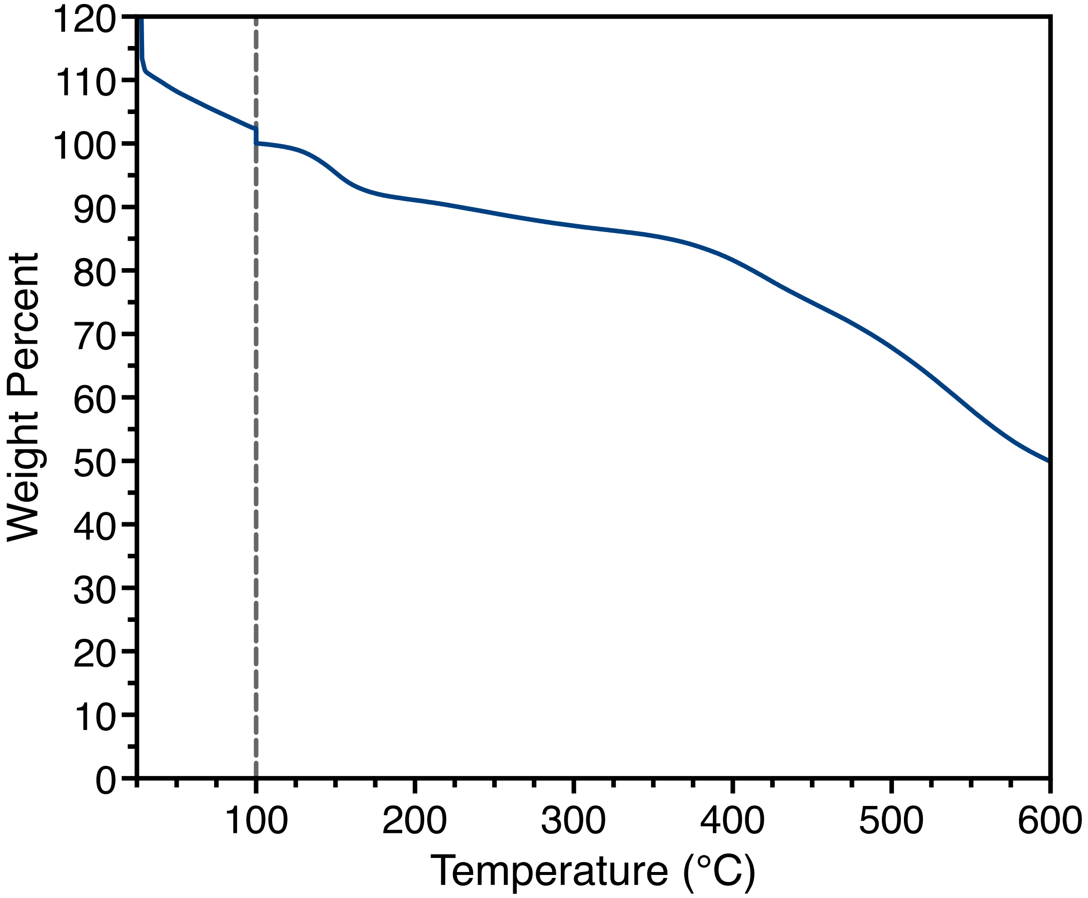

Figure S20. Thermogravimetric analysis of a slurry of **1**$(NiBr_2)_6$ in n-hexane. The sample was heated at a ramp rate of 1 °C/min. to 100 °C, then held at this temperature for 1 hour (dashed gray line) to evaporate any remaining n-hexane. The sample was then heated at a ramp rate of 1 °C/min. to 600 °C.

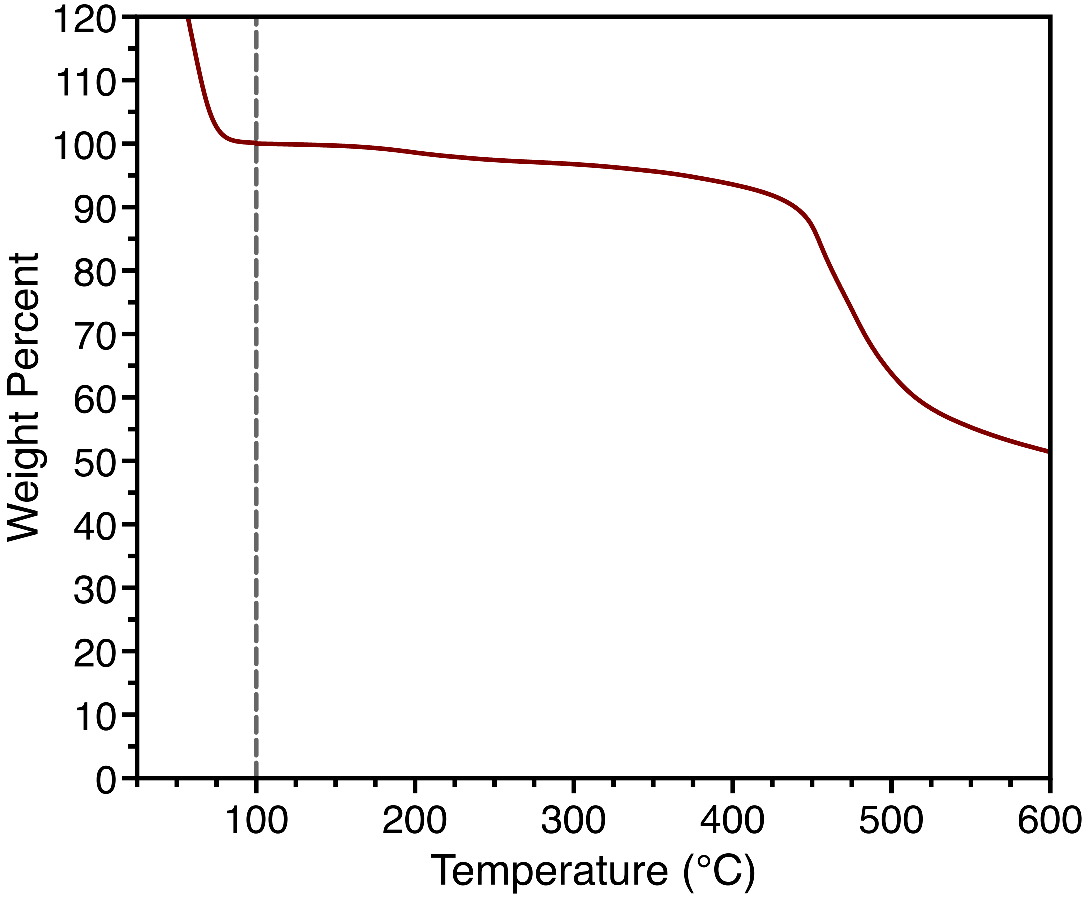

Figure S21. Thermogravimetric analysis of a slurry of **2**$(NiBr_2)_{0.84}$ in n-hexane. The sample was heated at a ramp rate of 1 °C/min. to 100 °C, then held at this temperature for 1 hour (dashed gray line) to evaporate any remaining n-hexane. The sample was then heated at a ramp rate of 1 °C/min. to 600 °C.

Ethylene Oligomerization Data

Table S3. Amount of $C_{4–18}$ oligomers produced from ethylene oligomerization reactions catalyzed by $1(NiBr_2)_6$, $2(NiBr_2)_6$, and $3(NiBr_2)_{0.14}$.

ethylene oligomer	**$1(NiBr_2)_6$**			**$2(NiBr_2)_{0.84}$**			**$3(NiBr_2)_{0.14}$**		
	mol%[ab]	**wt%[a]**	**α-olefin%[a]**	**mol%[ab]**	**wt%[a]**	**α-olefin%[a]**	**mol%[ab]**	**wt%[a]**	**α-olefin%[a]**
C_4	37(4)	5.0(9)	68(22)	77(9)	48(6)	48(8)	75(8)	60(11)	49(10)
C_6	28.2(8)	5.7(4)	56(26)	19(7)	18(7)	19(6)	21(6)	25(9)	26(17)
C_8	14(2)	3.8(2)	85(4)	3(2)	4(2)	31(14)	3(2)	6(4)	19(15)
C_{10}	7.5(1)	2.5(2)	88(4)	0.8(4)	1.3(6)	38(17)	0.6(5)	1(1)	13(2)
C_{12}	5.1(5)	2.1(2)	85.0(4)	0.30(1)	0.57(3)	50(21)			
C_{14}	3.6(3)	1.7(1)	83.0(8)	0.19(2)	0.41(1)	47(24)			
C_{16}	2.6(3)	1.4(1)	85.0(4)	0.11(3)	0.3(1)	49(24)			
C_{18}	2.0(2)	1.2(1)	86.0(7)	0.06(3)	0.2(1)	49(17)			

[a]Determined as an average of three replications. [b]Calculated for the $C_{4–18}$ product fraction.

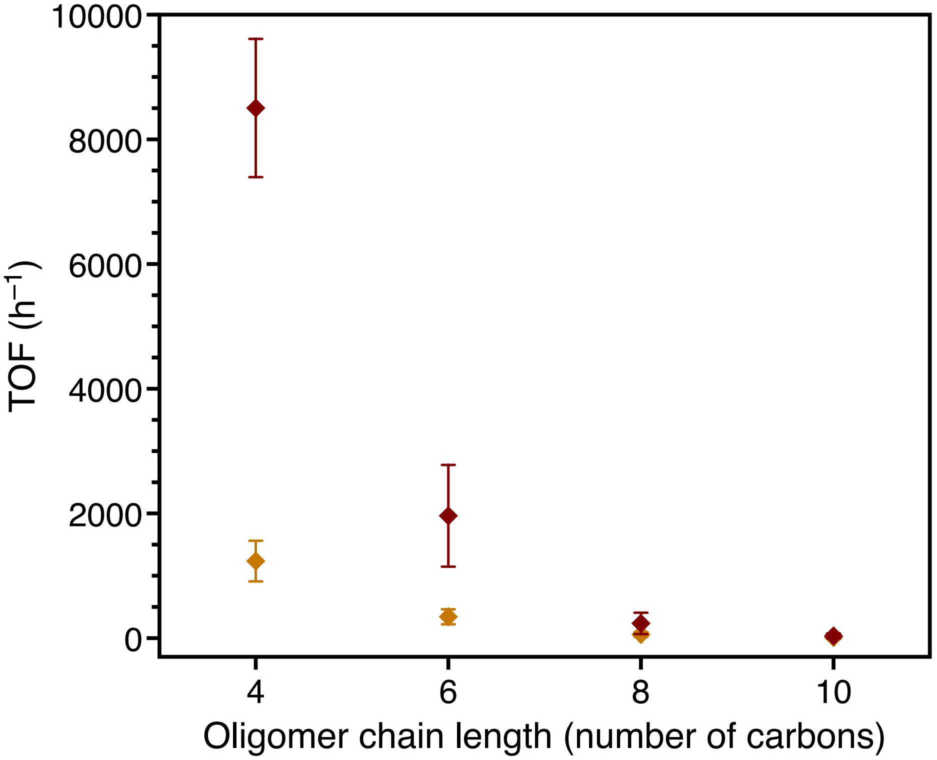

Figure S22. Comparison of the non-Schulz-Flory contribution to the average turnover frequencies ($mol_{oligomer}$ mol_{Ni}^{-1} h^{-1}) for $C_{4–10}$ oligomers produced in **2**($NiBr_2$)$_{0.84}$ (red) and the estimated average turnover frequencies for oligomers generated from adventitious nickel sites in **2**($NiBr_2$)$_{0.84}$ (yellow orange), assuming that **2**($NiBr_2$)$_{0.84}$ contains the same number of adventitious sites per zirconium as **3**($NiBr_2$)$_{0.14}$ (~17% of the nickel sites in **2**($NiBr_2$)$_{0.84}$).

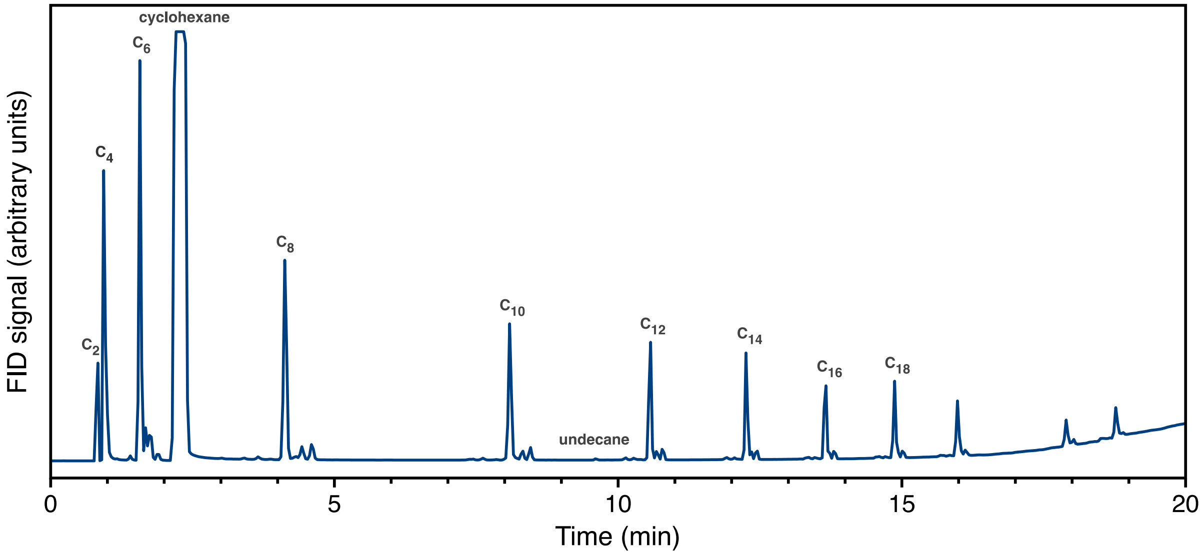

Figure S23. Representative gas chromatogram for the product mixture obtained from ethylene oligomerization catalyzed by **1**($NiBr_2$)$_6$.

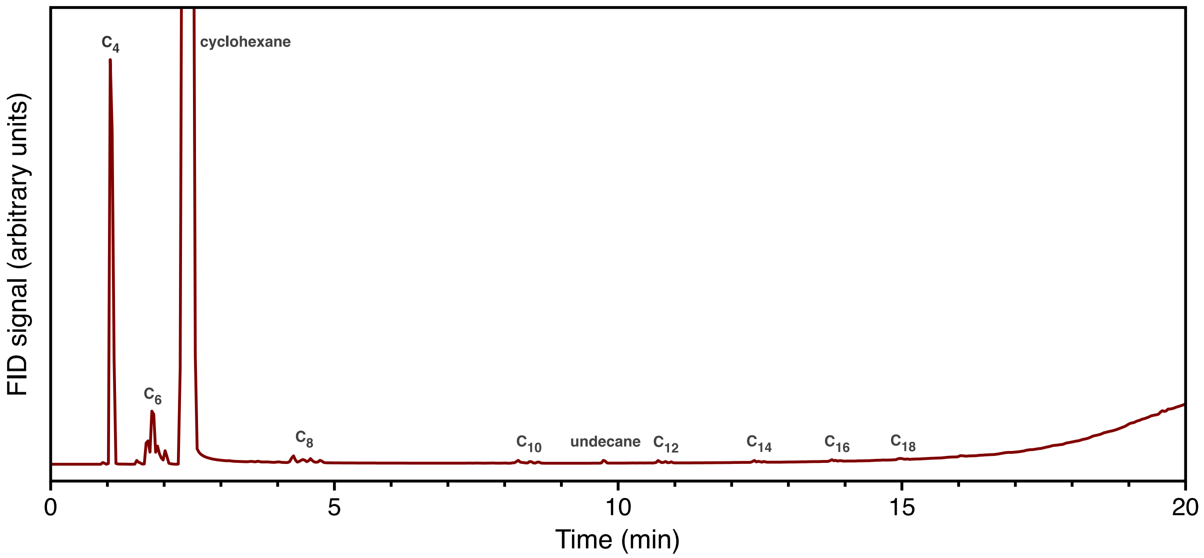

Figure S24. Representative gas chromatogram for the product mixture obtained from ethylene oligomerization catalyzed by **2**$(NiBr_2)_{0.84}$.

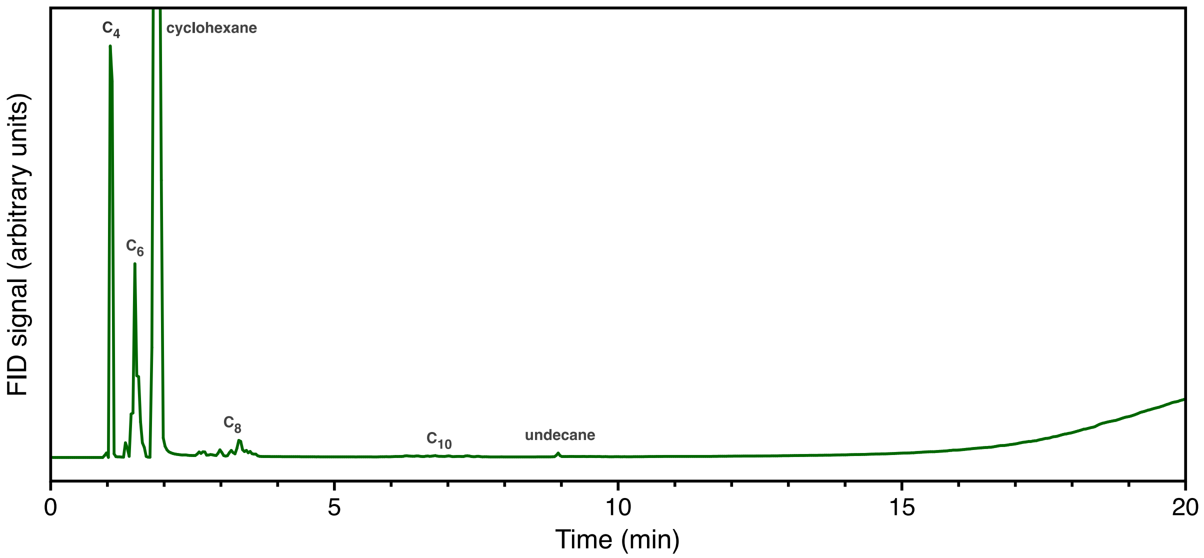

Figure S25. Representative gas chromatogram for the product mixture obtained from ethylene oligomerization catalyzed by **3**$(NiBr_2)_{0.14}$.

Scanning Electron Microscopy Images

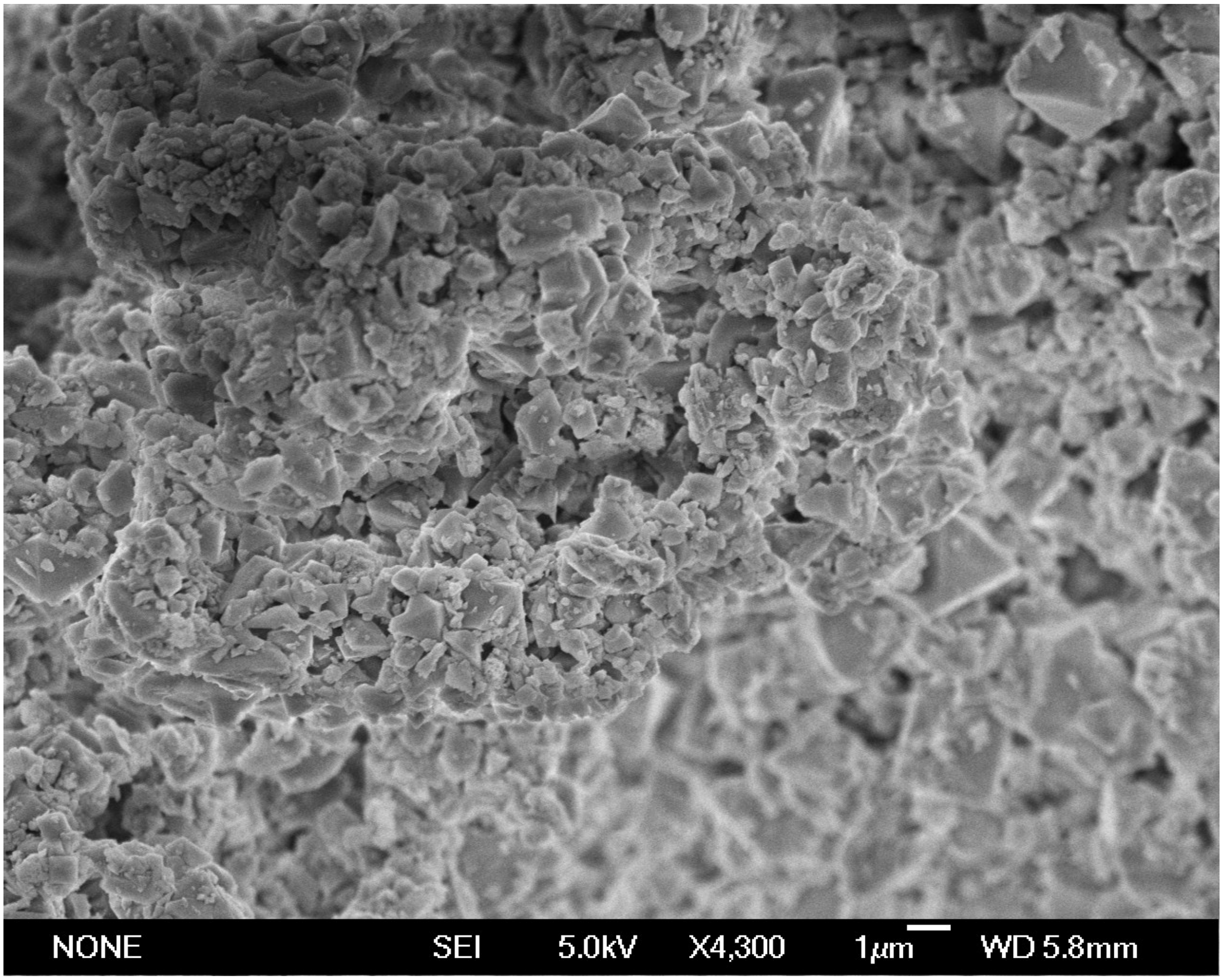

Figure S26. SEM micrograph of **1**($NiBr_2$)$_6$ (bulk sample).

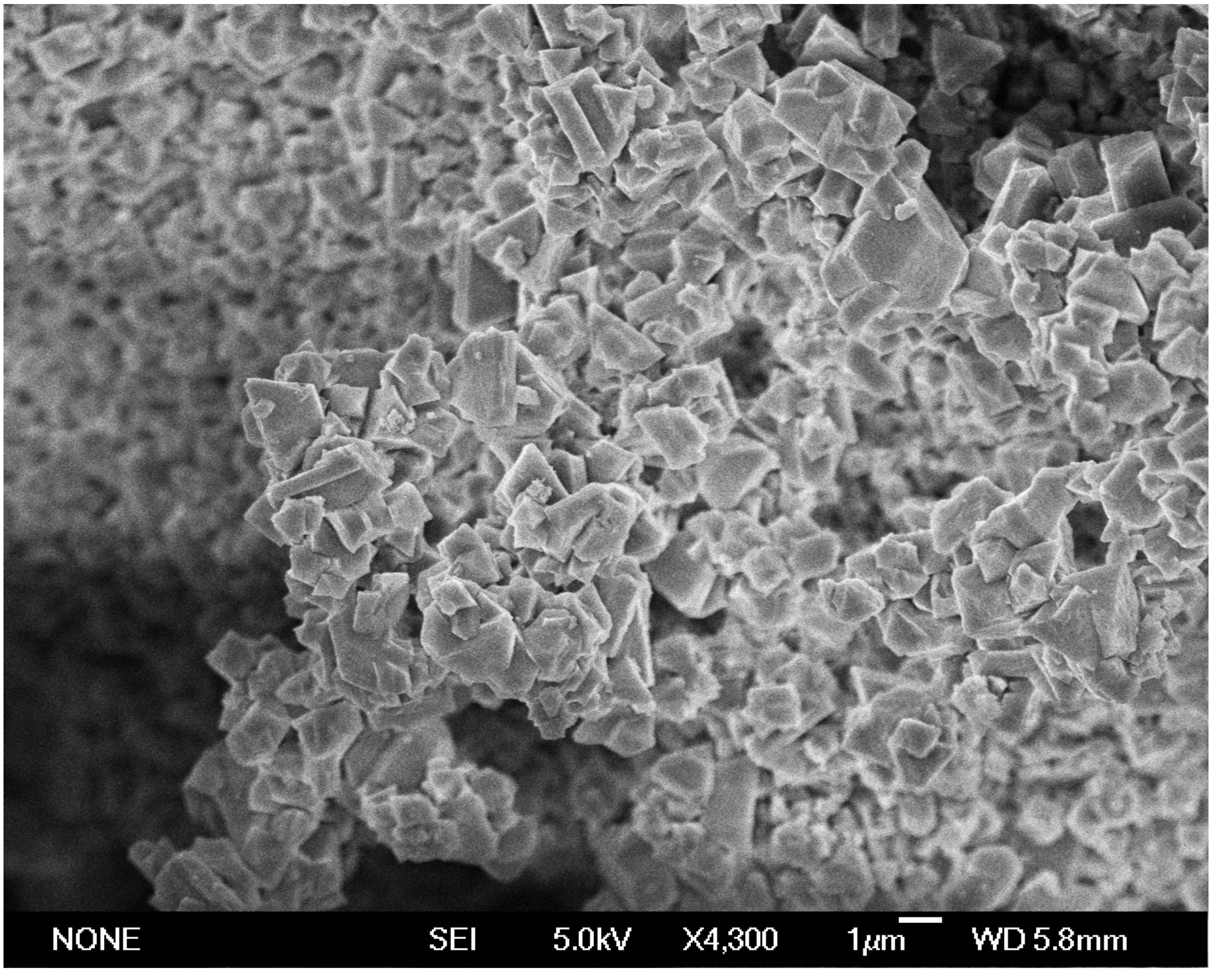

Figure S27. SEM micrograph of **2**$(NiBr_2)_{0.84}$.

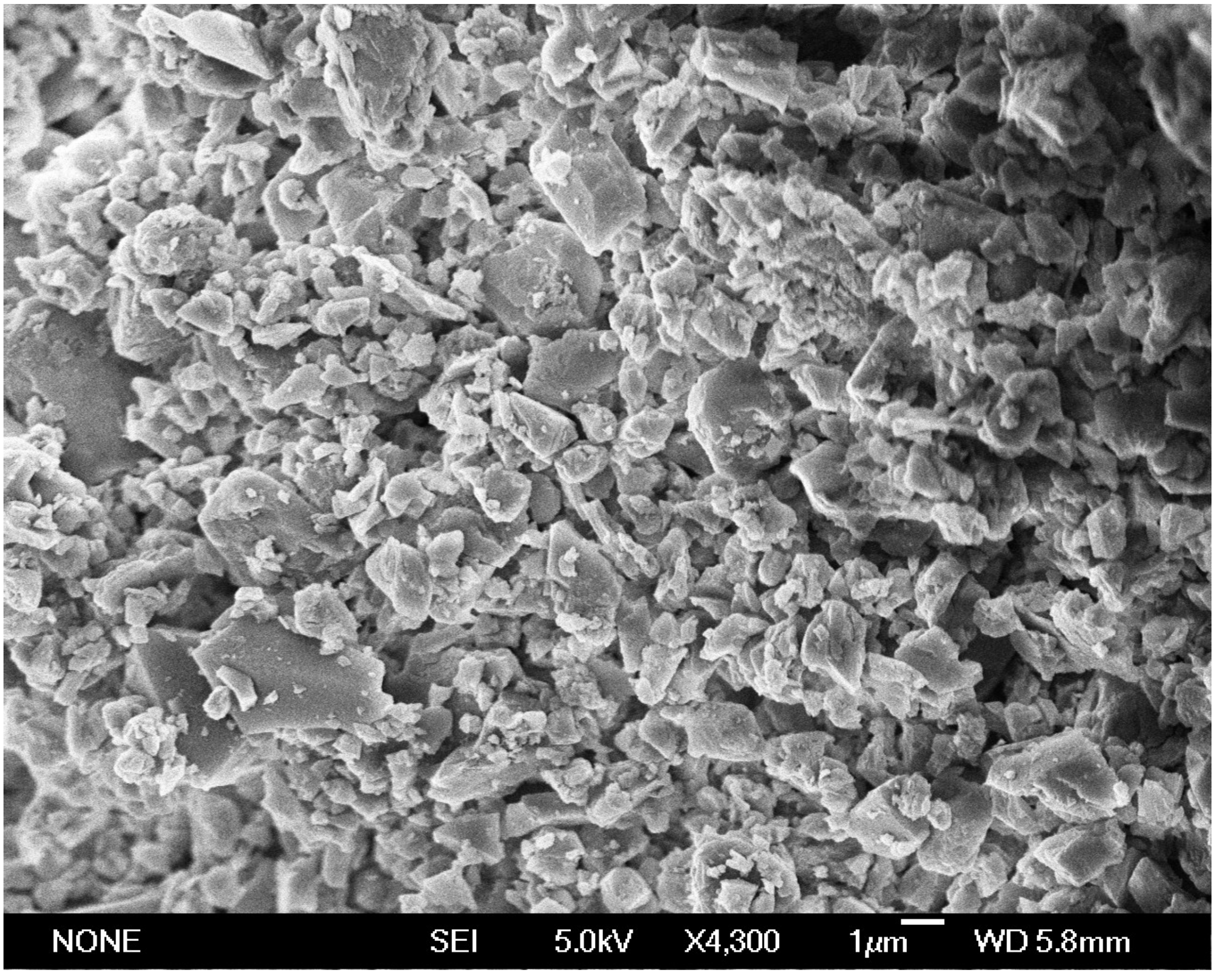

Figure S28. SEM micrograph of **3**$(NiBr_2)_{0.14}$.

Supplementary Experimental Methods

General procedure for metal content analysis via ICP-OES. Roughly 10 mg of activated material was placed in a 20-mL plastic vial and digested with 10 μL of concentrated HF in 2 mL of dimethylsulfoxide and diluted with 18 mL of 5% HNO_3 in Millipore water. The resulting solution was transferred to a 100-mL volumetric flask and diluted to mark with 5% (v/v) aqueous HNO_3 in Millipore water to give a stock solution that contained roughly 25 ppm Zr from the sample. The stock sample solution (10 mL) and 2.5 ppm Y (1 mL) were added to a 25-mL volumetric flask and diluted to mark with 5% (v/v) aqueous HNO_3 to give sample solution that is roughly 10 ppm Zr with 0.1 ppm Y as an internal standard. Standard solutions with 0.1, 1, 5, 10, and 15 ppm Zr and Ni with 0.1 ppm Y as an internal standard were prepared for the calibration curve.

References

1 A. A. Coelho, *TOPAS-Academic, Version 4.1*, Coelho Software, Brisbane, 2007.
2 K. S. Walton and R. Q. Snurr, *J. Am. Chem. Soc.*, 2007, **129**, 8552–8556.